C. R. Chimie 20 (2017) 181–189

Contents lists available at ScienceDirect

Comptes Rendus Chimie

www.sciencedirect.com

Full paper/Mémoire

Application of solar light for photocatalytic degradation of Congo red by a floating salicylic acid-modified TiO_2/palm trunk photocatalyst

Mouheb Sboui [a, b, *, 1], Mohamed Faouzi Nsib [b, c], Ali Rayes [b, c], Tsuyoshi Ochiai [d, e, **, 1], Ammar Houas [b, f]

[a] University of Sfax-Faculty of Science-Laboratory CI-Sfax, Tunisia
[b] URCMEP (UR11ES85), Faculty of Sciences, University of Gabès, 6029 Gabès, Tunisia
[c] National School of Engineers (ENIG), University of Gabès, 6029 Gabès, Tunisia
[d] Kanagawa Academy of Science and Technology, KSP building East 407, 3-2-1 Sakado, Takatsu-ku, Kawasaki, Kanagawa 213-0012, Japan
[e] Photocatalysis International Research Center, Tokyo University of Science, 2641 Yamazaki, Noda, Chiba 278-8510, Japan
[f] Al Imam Mohammad Ibn Saud Islamic University (IMSIU), College of Sciences, Department of Chemistry, Riyadh 11623, Saudi Arabia

ARTICLE INFO

Article history:
Received 10 October 2015
Accepted 15 December 2015
Available online 2 March 2016

Keywords:
TiO_2 nanoparticles
Floating catalyst
Salicylic acid
Surface modification
Photodegradation
Solar light

ABSTRACT

In this study, a highly active, low cost, simple and robust floating photocatalyst based on salicylic acid (SA)-modified TiO_2 immobilized on small pieces of palm trunk (PT) as a new porous and light weight support has been studied. These catalysts show the unique feature of floating on the water surface where optimum illumination and oxygenation occurs, leading to a strong increase in their photocatalytic efficiency. XRD, SEM, TGA, FTIR and DRS UV–Vis techniques were used to characterize the TiO_2–SA nanocomposite. Photocatalytic tests were carried out under solar irradiation and constrained conditions, i.e. non-stirring and non-oxygenation. The dye Congo red (CR) was used as a probe molecule. The obtained results showed that modification of the surface of TiO_2 nanoparticles by SA improved their photocatalytic activity. Particularly, TiO_2–SA (50 wt%)/PT was found to be very active whereas the unmodified TiO_2 nanoparticles sink to the bottom of the reactor and remain inactive due to the poor illumination and oxygenation. The prepared photocatalysts can be easily recovered, and their photocatalytic activity was found to be sustained after four consecutive runs.

1. Introduction

In the last decade, much attention has been paid to the eradication of various environmental pollutants such as dyes, pesticides, detergents, and volatile organic compounds from wastewater [1–4]. Traditional physical techniques such as adsorption on activated carbon, reverse osmosis, coagulation by chemical agents, and ion exchange on synthetic adsorbent resins, have been used for the removal of pollutants [5,6]. However, these methods only succeed in transferring organic pollutants from water to the

* Corresponding author. University of Sfax-Faculty of Science-Laboratory CI-Sfax, Tunisia.
** Corresponding author. Kanagawa Academy of Science and Technology, KSP building East 407, 3-2-1 Sakado, Takatsu-ku, Kawasaki, Kanagawa 213-0012, Japan.
E-mail addresses: sboui.mouheb@gmail.com (M. Sboui), pg-ochiai@newkast.or.jp (T. Ochiai).
[1] These authors contributed equally to this work.

http://dx.doi.org/10.1016/j.crci.2015.12.007
1631-0748/

solid phase. Further, secondary pollution is created, which entails additional and costly solid-waste treatment and regeneration of the adsorbent. Therefore, an alternative to conventional methods is needed. In this regard, photocatalysis, as an advanced oxidation process, is one of the promising alternative methods applied in this field.

It is based on the photogeneration of reactive species such as hydroxyl radicals (•OH) which can oxidize a broad range of organic pollutants quickly and non-selectively [7]. Due to its high chemical stability, non-toxicity, high photocatalytic activity to oxidize pollutants in air and water, and relatively low price, TiO_2 has been widely used as a photocatalyst in recent decades [8–11]. However, its application is limited because of its narrow photocatalytic region (near-ultraviolet region) and small absorption fraction (<5%) of incident solar irradiation and indoor light [12–14].

Moreover, the extreme low coverage of organic pollutants on the TiO_2 surface is another limitation of the low photocatalytic efficiency [15,16].

To improve the affinity between organic pollutants and the TiO_2 surface, aromatic carboxylic acids such benzoic (BA) and salicylic (SA) acids are usually used as surface modifiers. Particularly, the TiO_2 surface modification by SA may enhance the surface coverage of organic pollutants, expand the wavelength response range and improve the dispersive capacity of TiO_2 powder in polar and non-polar solvents [17].

Carboxylic acid-modified TiO_2 photocatalysts are always bulk particles or powder materials [18–21]. They always sink or suspend into the solution leading to a reduction in the fraction of sunlight used in the photocatalytic reaction. Furthermore, a common drawback of suspended catalysts is the difficulty associated with the recycling, which usually limits their practical applications. In this paper, a new concept is developed called the “floating photocatalyst” to solve the above limitations. The designed floating photocatalyst consists of surface-modified TiO_2 immobilized on a floatable substrate (Scheme 1). The floatable photocatalysts are especially interesting for solar remediation of non-stirred and non-oxygenated reservoirs since the process maximizes: (i) the illumination/light use (due their ability to float), and (ii) the oxygenation of the photocatalyst due to the proximity to the air/water interface. The optimization of illumination and oxygenation should result in higher rates of radical formation and oxidation efficiency. Floating photocatalysts can be applied for local solar remediation, i.e. directly in the contaminated wastewater reservoirs located in remote areas without any special equipment or installation. Also, they can be used for more efficient destruction of suspended insoluble organic contaminants, e.g., in oil-spill accidents [22]. Palm trunk PT is a natural material of low density, antistatic properties and heat insulation. So, it can be used efficiently as a floating substrate. PT is a suitable support for photocatalytic applications since it is an innocuous material with good chemical, mechanical and thermal stability. Moreover, PT is a hydrophobic material and can pre-concentrate organics from water on its surface improving the removal and oxidation efficiency. PT with a highly developed porous structure formed by the inter-lamellar space has been used for different applications as an adsorbent and absorbent.

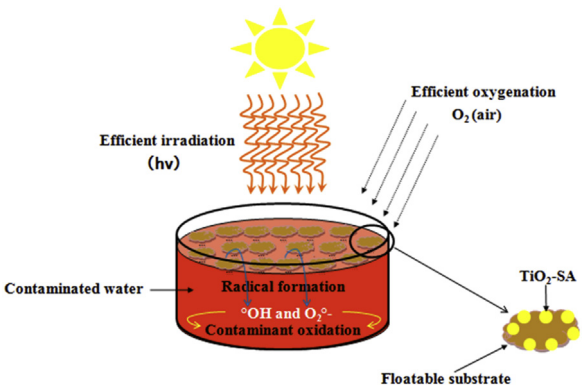

Scheme 1. Schematic representation of the floating photocatalyst used for the oxidation of CR dye.

The aim of this research work is then to prepare a TiO_2–SA/PT as a floating photocatalyst and to examine its efficiency in photodegradation of pollutants under solar light and constrained conditions (non-stirring and no artificial oxygenation).

2. Materials and methods

2.1. Materials

All reagents used were of analytical grade and employed as received. Titanium tetraisopropoxide (TTiP) and sodium dodecyl sulfate (SDS) were purchased from Aldrich Chemicals. Ethanol, salicylic acid (SA) and acetic acid were obtained from Merck Chemicals. The azo dye used in the experiments is Congo red (CR). PT was obtained from palm oases of Gabes (Tunisia).

2.2. Preparation of the TiO_2 photocatalyst

The TiO_2 photocatalyst was prepared through the sol–gel process. The two precursor solutions, here denoted as precursors A and B were prepared as follows. Precursor A: TTiP (22.5 mL), ethanol (50 mL) and acetic acid (3.0 mL). Precursor B: H_2O (27.0 mL), ethanol (50 mL) and SDS (0.43 g). Each precursor was stirred for 10 min at room temperature. Afterwards, precursor B was added to precursor A dropwise with vigorous stirring. The resultant mixture was further stirred for 20 min. The sol solution was placed in a culture dish for 1.0 day to finish the sol–gel transition and filtered. The filter residue was rinsed with water repeatedly, and then dried at 110 °C for 24 h to obtain a dried gel. The dried gel was ground and heat treated at 350 °C for 6.0 h to get a stable TiO_2 photocatalyst.

2.3. Surface modification

Surface modification was carried out through adding 1.0 g of the TiO_2 nanoparticles into 50 mL of saturated solution of SA. A constant magnetic stirring was conducted

for 30 min at room temperature until the adsorption equilibrium, resulting in a light yellow coloration of the surface of TiO_2, inferring that a chemical reaction took place (chemisorption) between SA and TiO_2. After being filtered, the surface-modified titania nanoparticles (TiO_2–SA) were washed with water three times and heat treated for 30 min at 105 °C. The obtained powder was then ground to get fine particles.

2.4. TiO_2–SA/PT photocatalyst preparation

The floating photocatalysts TiO_2–SA/PT were prepared from a suspension of TiO_2–SA on the PT surface. The PT was divided into small pieces. Different TiO_2–SA contents of 50, 70 and 100 wt % were used. The immobilization of the photocatalysts on PT pieces was performed under vigorous stirring at room temperature; by dissolving 3.0 mL of binder in 30 mL distilled water containing 1 g of PT. Then, an appropriate amount of TiO_2–SA was added. The resultant mixture was further stirred vigorously for 30 min. After filtration, the recovered product is dried in an oven at 60 °C for 5.0 h. The TiO_2–SA/PT beads were subsequently subjected to vigorous stirring in water for 2.0 h to remove any TiO_2–SA particle loosely attached to the PT surface.

2.5. Catalyst characterization

The TiO_2 nanoparticles and TiO_2–SA nanocomposites were characterized by X-ray diffraction (XRD), scanning electron microscopy (SEM), thermogravimetric analysis (TGA), Fourier transform infrared spectroscopy (FTIR), and diffuse reflectance spectroscopy (DRS). The XRD patterns obtained on a D5000X-ray diffractometer (German Bruker) using Cu Kα radiation at a scan rate of 0.02° s^{-1} were used to decide the crystallite size and identity of TiO_2 powders. The average crystallite size was determined according to Scherrer's equation:

$$d = \frac{K\lambda}{\beta cos\theta}$$

where k is the shape factor of particles equal to 0.89, β is the peak width at half maximum (in radians), λ is the X-ray wavelength (0.15418 nm), and θ is the Bragg angle. The SEM was recorded with a Neoscope JCM-5000 (JEOL Company, Japan) electron microscope and was used for observing the shape and morphology of the prepared particles. TGA experiments of the prepared pure TiO_2 and TiO_2–SA composites were performed with a SETERAM thermo-balance, under a dynamic atmosphere of argon. The samples were put into platinum crucibles, at a heating rate of 10 °C min^{-1}. The modifying effect of TiO_2 nanoparticles with salicylic acid and their stability during photocatalysis was characterized by using a PerkinElmer SPECTRUM 1000 Fourier transform infrared (FTIR) spectrometer in the range 200–4000 cm^{-1} with 32 scans through the FTIR curves. The powders of pure and modified TiO_2 were prepared as pellets containing 0.3 mg of material mixed with 30 mg of KBr. A UV–Vis 3101 PC (UV Probe Shimadzu) was used to record the DRS of the samples. Reflectance spectra were analyzed under ambient conditions in the wavelength range of 200–800 nm.

2.6. Photocatalytic experiments

A special photocatalytic reactor of 250 mL with an outside diameter ($\varnothing_{out} = 90$ mm), height ($H = 45$ mm) and covered walls was designed to produce only surface illumination avoiding lateral light incidence. The reactions were carried out under natural sunlight irradiation (out in the city of Gabes, in the month of July between 10 am and 2 pm). The photocatalytic studies were carried out with the reactive textile dye CR as a probe molecule at 10 mg L^{-1} concentration. Before the reaction, the catalyst was kept in the dye solution (100 mL, 10 mg L^{-1}) in the dark for 60 min to reach adsorption equilibrium. No stirring was used in the reactions in order to avoid oxygenation of the solution and to simulate the use of a floating photocatalyst. During the photodegradation process, the samples were collected every 30 min, and the catalyst was removed by centrifugation. An UV–Vis spectrometer (UV-2550, Shimadzu, Japan) was used to measure the organic dye concentration before and after degradation. The degradation efficiency (D) was calculated using the following equation [23,24].

$$D = \frac{C_0 - C_e}{C_0} \times 100\ (\%)$$

where C_0 is the initial concentration of target organic dye solution (mg L^{-1}) and C_e is the equilibrium concentration after degradation (mg L^{-1}).

3. Results and discussion

3.1. XRD analysis

XRD analysis of the prepared pure TiO_2 and modified TiO_2–SA nanocomposites (Fig. 1) was conducted to investigate the influence of SA deposition on the crystalline phase of TiO_2 nanoparticles. Fig. 1a reveals a unique anatase solid phase characterized by the principal peaks observed

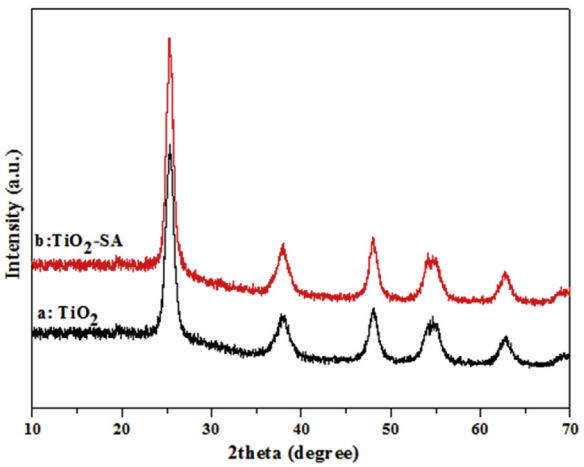

Fig. 1. XRD patterns of the prepared pure TiO_2 (a) and modified TiO_2–SA nanocomposites (b).

at $2\theta = 25.3$, 37.9, 48.1, 54, 55.2 and 62.8° which exactly match (101), (004), (200), (105), (211) and (204) reflections of the pure anatase phase. The characteristic peaks of rutile and brookite phases are not observed, revealing that these phases do not exist in the as-prepared TiO_2. Fig. 1b shows that the modification of the TiO_2 particles by SA does not cause any change in their peak positions and shapes compared to TiO_2. This indicates that SA modification through impregnation at room temperature does not change the crystalline structure of TiO_2. The average crystallite size of TiO_2 and TiO_2–SA particles, calculated using Scherrer's equation is found to be equal to 5.22 nm and 5.16 nm, respectively. Broad diffraction peaks are due to the small crystalline size of TiO_2–SA particles.

3.2. SEM images

SEM images were recorded for unmodified TiO_2 and TiO_2–SA nanocomposites to investigate the effect of surface modification on the morphology and aggregation level of nanoparticles (Fig. 2). The SEM images show that TiO_2 particles are more aggregated than the modified TiO_2–SA ones. The average size of TiO_2 aggregates is 1 μm (Fig. 2a). The synthesized TiO_2–SA nanoparticles appear less aggregated, small in size and have a spherical-like shape with a uniform size distribution (Fig. 2b). A higher dispersion increases the specific surface area, which ultimately enhances the photocatalytic performance on the TiO_2–SA nanopowders.

3.3. Thermal stability

The amount of SA adsorbed on the TiO_2 surface was deduced from thermogravimetric analysis of prepared pure TiO_2 and TiO_2–SA nanocomposites (Fig. 3). The TGA curve of the prepared pure TiO_2 (Fig. 3a) shows thermal stability up to 500 °C where the loss of mass is negligible (1%) and may due to some humidity. A larger mass loss of about 4% is registered with the TiO_2–SA nanocomposite (Fig. 3(b)) and corresponds to the decomposition of the adsorbed SA. As expected, the nanocomposite TiO_2–SA has become more resistant to thermal degradation, probably because of the strong interactions between the TiO_2 and SA.

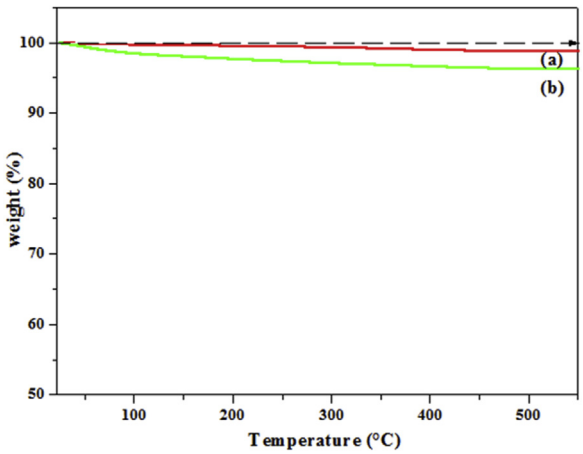

Fig. 3. TGA curves of (a) prepared pure TiO_2 and (b) modified TiO_2–SA nanocomposites.

3.4. FTIR analysis

Fig. 4 depicts the FTIR spectra of the prepared TiO_2 powders before (a) and after (b) modification. The FTIR spectrum of pure TiO_2 shows the deformation frequencies of OH functions of adsorbed water located at 1674 and 3462 cm^{-1}. The peak located at 1111 cm^{-1} is attributed to the stretching vibration of the Ti–OH bond whereas the absorption peak at 576 cm^{-1} is a characteristic of the Ti–O bond vibration [25]. The spectrum of TiO_2 modified by salicylic acid (TiO_2–SA) shows new peaks allocated to C=O of the ester group (1711 cm^{-1}), phenyl (1441 and 1474 cm^{-1}) group and –COOTi– group (1385 cm^{-1}). This result suggests the formation of a fairly stable complex between Ti^{IV} surface ions and salicylic acid. The formation of this complex is also shown by the appearance of a yellow coloration on TiO_2 particles that can be explained as a result of a ligand to metal charge transfer transition. Indeed, salicylic acid shows a great affinity to Ti^{IV} ions in solution and chemisorbs efficiently at the titanium dioxide surface. The combination of a –OH group and a –COOH group at ortho positions of the benzene ring infers some strong

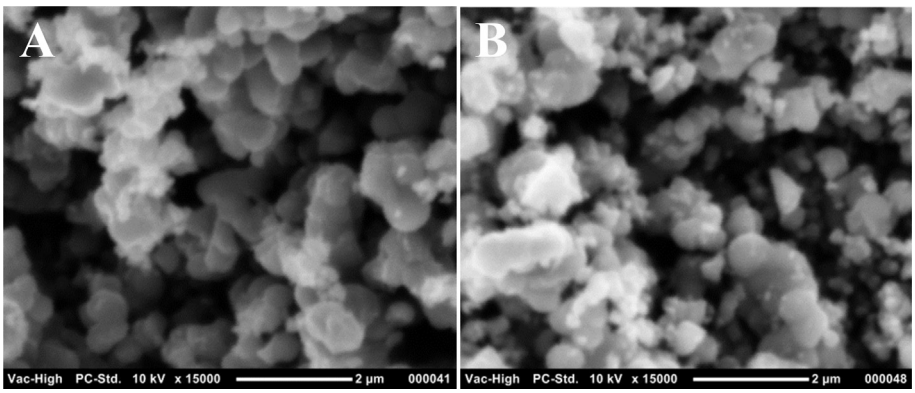

Fig. 2. SEM images of (A) prepared pure TiO_2 and (B) modified TiO_2–SA nanocomposites.

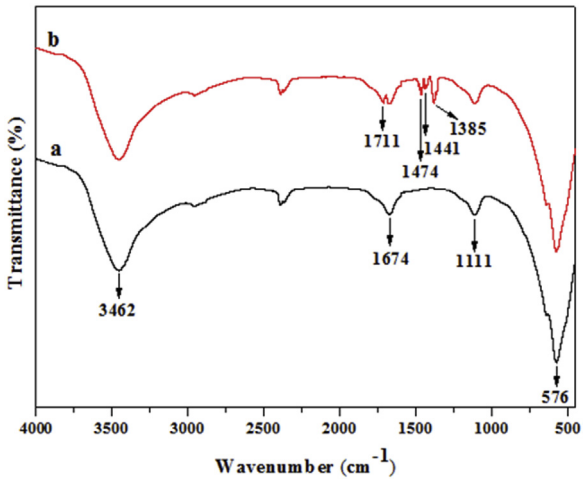

Fig. 4. FTIR spectra of (a) prepared pure TiO_2 and (b) modified TiO_2–SA nanocomposite.

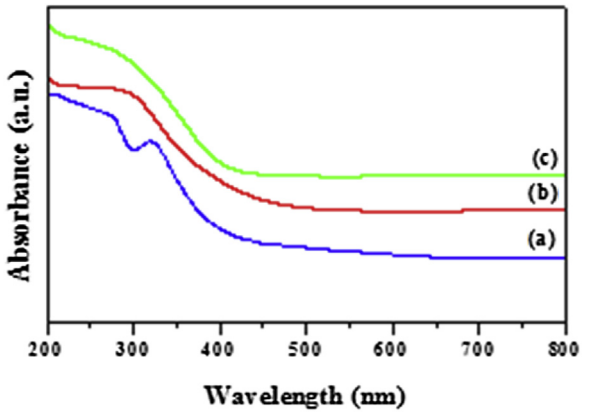

Fig. 5. UV–Vis diffuse reflectance spectra of (a) pure SA; (b) prepared pure TiO_2 and (c) modified TiO_2–SA nanocomposite.

interaction between the salicylic acid and the TiO_2 particle surface. The dissociation constants of salicylic acid are $pK_{a1} = 2.81$ and $pK_{a2} = 13.4$. As a result, the –COOH group of salicylic acid is dissociated into $-COO^-$ and H^+. The Ti^{IV} surface ions of the TiO_2 typically bond with the oxygen atoms of water molecules. However, in the presence of salicylate anions in solution, the –COOH and the –OH groups form chelate surface structures with the surface Ti^{IV} ions leading to the replacement of water by the organic ligand [26]. Two structures of the surface complexes are proposed: bidentate chelating and less stable bidentate bridging, or monodentate through the oxygen atom of the carboxyl group [27–29]. A chelating bidentate surface salicylate species, coordinated via a C–O bond of the carboxylate group, is the most likely resulting structure at the TiO_2 surface [30]. Shun-Xing [17] established that salicylic acid and –OH groups on the TiO_2 surface interact through the esterification reaction leading to the formation of ester with a stable six-membered ring. The formation of such a surface complex TiO_2–SA can lead to a shift of absorption edge toward the visible spectrum up to 430 nm.

3.5. DRS analysis

Fig. 5 shows the DRS of the prepared pure TiO_2 and modified TiO_2–SA nanocomposite. It is obvious that pure TiO_2 absorbs only light with wavelengths below 380 nm. However, the modified TiO_2–SA nanocomposite exhibits strong absorption in the visible range (from 400 to 800 nm), which conforms to the light yellow color of the powder. Notably, the absorption edge of the TiO_2–SA red-shifts about 40 nm compared to that of the neat TiO_2 sample. The DRS result indicates that electron transfer between SA and TiO_2 nanoparticles exists in TiO_2–SA, which might be favorable for the improvement of the photocatalytic activity of TiO_2. The band gap energies (E_g) of the pure TiO_2 and modified TiO_2–SA nanocomposite were 3.2 and 2.9 eV, respectively. The band gap energies of the photocatalysts were determined using the following equation: E_g (eV) = 1239.8/λ [31], where λ is the wavelength (nm). The above results show that SA is capable of sensitizing TiO_2 efficiently. Consequently, the TiO_2–SA nanocomposite can be excited to produce much more electron–hole pairs under visible light illumination, resulting in higher photocatalytic activities. This also shows that SA modification provides an effective approach to extend the absorption of TiO_2 to the visible light range.

3.6. Effect of solution pH

The pH of the solution is a vital parameter in the photodegradation of organic dyes because it determines the surface charge of the photocatalyst, the electrostatic interaction between the photocatalyst surface and organic dye molecule, and the number of charged radicals generated during the photocatalytic oxidation process [32]. In addition, the initial solution pH may affect the aggregation of the particles and the conduction and valence band positions of the catalyst. To decide the effect of the pH value of organic dye solution on the photocatalytic performance, a series of comparative photodegradation of CR were performed in the presence of TiO_2–SA/PT, TiO_2/PT, TiO_2–SA and pure TiO_2 under solar light irradiation. The studies were carried out at a pH value ranging from 4 to 10. The pH of the solutions was adjusted with HCl or NaOH solution by using a pH meter.

Fig. 6 shows the degradation efficiency at different pH values. The maximum of the photocatalytic performance was acquired at pH = 6 for all the photocatalysts tested here. In particular, TiO_2–SA (50 wt %)/PT shows the highest degradation efficiency (84.2%) of CR after 100 min of irradiation. This result can be explained taking into account the charge surface state of TiO_2–SA and the ionic state of CR in the solution. CR molecules with two sulfonic groups ionize easily in strong acidic media and become a soluble CR anion, which can be easily adsorbed on TiO_2–SA particles with positive surface charge. So, the maximum degradation ability of TiO_2–SA/PT under solar light was measured under the optimum experimental conditions: concentration of the organic dye (CR) = 10 mg L^{-1} and pH = 6.

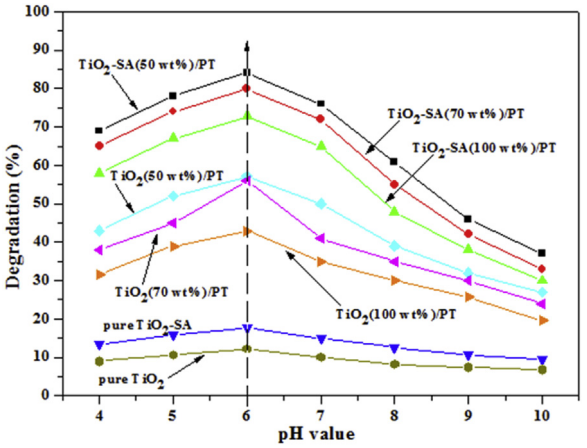

Fig. 6. Effect of pH values on the photodegradation of CR after 100 min (Experiments were carried out under solar light irradiation, T = 34 ± 2 °C, Volume = 100 mL; initial concentration of CR = 10 mg L^{-1}; catalyst dose = 1.0 g L^{-1}).

3.7. Photodegradation of CR

Fig. 7 shows the concentration variation of CR solution when irradiated with solar light in the presence of different catalysts. Before photocatalytic tests, the dye solution was left in contact with the photocatalyst for 1.0 h in the dark to reach the adsorption equilibrium. The blank test (in the absence of catalyst) reveals that the decrease of the CR concentration due to its photosensitization property is not significant. Besides, Fig. 7 shows that the adsorption potential of SA- modified TiO_2 is higher than that of the unmodified TiO_2. According to the SEM and DRS studies, the TiO_2–SA particles have a small size compared to pure TiO_2, resulting in a higher surface area. Thus, TiO_2–SA provides more sites for the adsorption and the removal of the organic molecules.

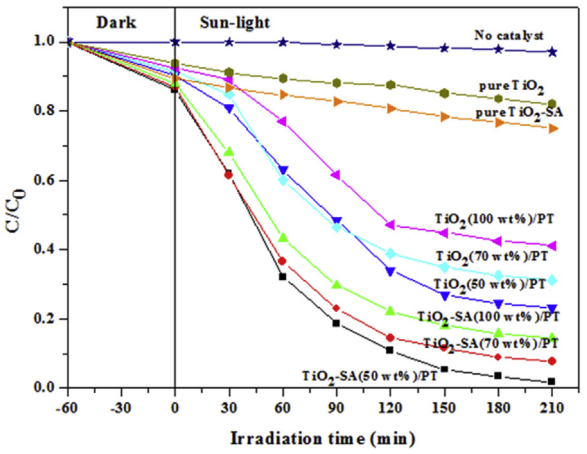

Fig. 7. Photocatalytic degradation curves of CR in the presence of different catalysts. (Experiments were carried out under solar light irradiation, $T = 34 \pm 2$ °C, volume = 100 mL; initial pH was used; initial concentration of CR = 10 mg L^{-1}; catalyst dose = 1.0 g L^{-1}.)

After Fig. 7 it is noticeable that the degradation efficiency of CR over TiO_2–SA was much higher compared to that over TiO_2. This result may be explained according the UV–Vis DRS spectra of pure TiO_2 and TiO_2–SA nanocomposite. As has been shown in Fig. 5, TiO_2–SA absorbs more visible light than pure TiO_2 due to its lower band gap energy. It is also remarkable that the degradation rate of CR became higher when the photocatalysts were supported on PT. The low activity of the non-supported photocatalysts is due to its deposition at the bottom of the reactor. On the other hand, the TiO_2–SA/PT catalysts showed high activities. However, as the TiO_2–SA content increases in the TiO_2–SA/PT composite the photocatalytic activity decreases. The same tendency was observed with the TiO_2/PT composites. This behavior may be due to the opacity caused by excess of the photocatalyst clusters. The presence of these clusters reduces light penetration and increases the scattering effect. Moreover, it leads to a very weak dispersion of the catalyst particles, a weak transfer material and a bad illumination.

Additionally, the maximum photocatalytic efficiency was achieved using TiO_2–SA (50 wt %)/PT to remove about 98.2% of the CR from the solution. The efficient photocatalytic activity of the TiO_2–SA (50 wt %)/PT floating photocatalyst under solar light irradiation resulted from the efficient illumination and oxygenation which are fundamental for the photocatalytic process. The optimization of illumination and oxygenation should result in higher rates of radical formation and oxidation efficiency.

The surface modification of TiO_2 by SA is advantageous in the photocatalytic process for the following reasons: First, the small size of particles and subsequently the high specific surface area of TiO_2–SA offer more adsorption sites and remarkably allow an increase of the local concentration of organic dye in the vicinity of the TiO_2 photoactive layer [33]. Second, the TiO_2–SA nanocomposite has a structure which could enhance the light-capturing efficiency by multiple reflections of light between the organic chelating ligands (SA). Third, the modification of the TiO_2 surface by SA decreases the rapid recombination rate of the photogenerated electron–hole and the radiative recombination rate of the self-trapped excitons.

3.8. Effect of the photocatalyst loading

Fig. 8 shows the effect of the amount of TiO_2–SA (50 wt %)/PT floating photocatalyst on the photodegradation efficiency of CR. It can be observed that as the amount of the photocatalyst increased the CR discoloration also increased. These results suggest that the TiO_2–SA content in PT has an important effect on the reaction kinetics. In particular, if the amount of TiO_2–SA (50 wt%)/PT was equal to 1.0 g·L^{-1}, the CR discoloration attained after 150 min of solar light irradiation was 94.6% without any stirring or oxygenation.

3.9. Effect of hydrogen peroxide

Hydrogen peroxide (H_2O_2) is an electron scavenger which may accept a photogenerated electron from the conduction band and thus prevents electron–hole recombination by forming •OH radicals [34]. For this reason, the

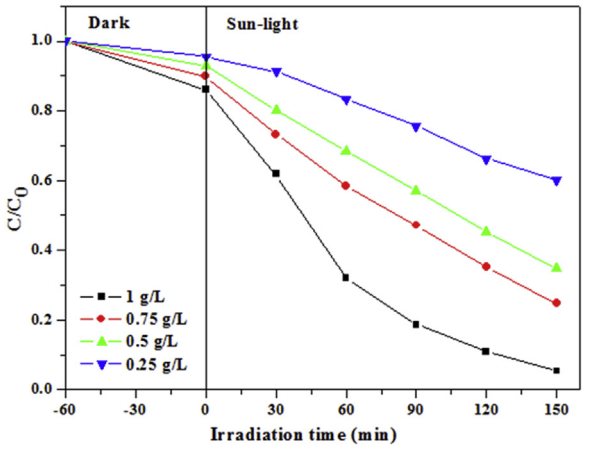

Fig. 8. Effect of the amount of TiO_2–SA (50 wt %)/PT floating photocatalyst on the discoloration of CR dye after 150 min. (Experiments were carried out under solar light irradiation, $T = 34 \pm 2$ °C, volume = 100 mL; pH: initial; initial concentration of CR = 10 mg L^{-1}.)

effect of H_2O_2 dosage, from 5 to 35 mM, on the photodegradation of CR was investigated in the presence of TiO_2–SA (50 wt %)/PT. As shown in Fig. 9, there was an optimal dosage of H_2O_2, 20 mM, at which the degradation efficiency of CR attained a maximum. Below the optimal dosage, the enhancement of the degradation efficiency by the addition of H_2O_2 could be attributed to the increase of reactive hydroxyl radical concentration [35]. The increase in the concentration of hydroxyl radicals resulting from the decomposition of H_2O_2 promoted the CR degradation process. Ohno et al. have reported that the interaction between H_2O_2 and TiO_2 leads to the formation of titanium peroxide complex TiO_2–H_2O_2 on the TiO_2 surface. The TiO_2–H_2O_2 complex extends the photoresponse of TiO_2 to the visible region, leading to the visible-light-induced surface electron transfer from the surface complex to the conduction band of TiO_2 [36]. The electrons on the conduction band of TiO_2

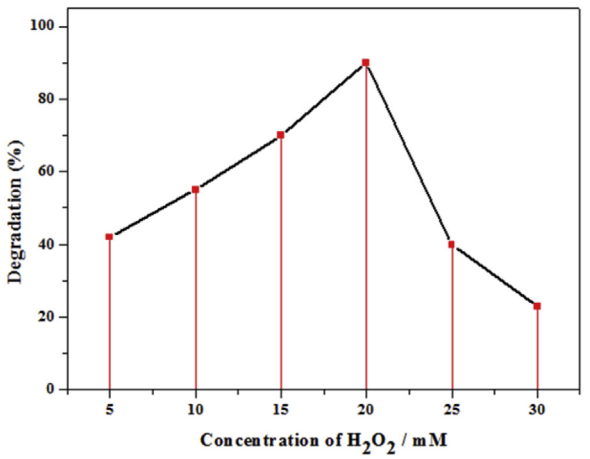

Fig. 9. Effect of dosage of H_2O_2 on the photodegradation of CR after 100 min in the presence of TiO_2–SA (50 wt %)/PT. (Experiments were carried out under solar light irradiation, $T = 34 \pm 2$ °C, volume = 100 mL; pH: natural; initial concentration of CR = 10 mg L^{-1}; catalyst dose = 1.0 g L^{-1}.)

initiate the decomposition of H_2O_2, which gives rise to the generation of hydroxyl radicals as follows [37]:

$$H_2O_2 + e^- \rightarrow {}^{\bullet}OH + OH^-$$

where e^- is the electron transferred from the surface complex to the conduction band of TiO_2.

H_2O_2 is expected to play a double role in the photocatalytic degradation process. On receiving a photogenerated electron from the conduction band of TiO_2, it promotes the charge separation and forms $^{\bullet}OH$ radicals as follows:

$$H_2O_2 + O_2 \rightarrow OH^- + {}^{\bullet}OH + O_2$$

When H_2O_2 was added at higher dosage, the degradation efficiency of CR decreased. This was because the very reactive $HO^{\bullet}$ radicals and the valence band holes could be consumed by H_2O_2 itself [38,39]. This negative effect of high concentration of H_2O_2 may be due to the formation of $HO_2^{\bullet}$, which is significantly less reactive than $HO^{\bullet}$. Thus, H_2O_2 acts as a powerful $HO^{\bullet}$ scavenger along with the photogenerated holes and inhibits the generation of $HO^{\bullet}$ radicals and thereby decreases the degradation rate as follows:

$$H_2O_2 + {}^{\bullet}OH \rightarrow H_2O + HO_2^{\bullet}$$

$$HO_2^{\bullet} + HO^{\bullet} \rightarrow H_2O + O_2$$

$$H_2O_2 + h^+ \rightarrow HO_2^{\bullet} + H^+$$

Therefore, the mechanism behind the photodegradation of organic compounds in the presence of the modified TiO_2/H_2O_2 system is still not well defined. The effect of H_2O_2 addition on the kinetics of degradation is not always positive and seems to depend on the studied system.

3.10. Photocatalyst reuse

The ability of a photocatalyst to be reused is one of the most important parameters which determines, from an economical point of view, the potential exploitation of a material in practical systems for water treatment. To examine the repeatability of the photocatalytic activity, the TiO_2–SA (50 wt %)/PT was used for four consecutive photodegradation cycles. The concentration of the organic compound (CR) was measured after 210 min of solar light irradiation (Fig. 10). After each cycle, the photocatalyst was rinsed, dried and used again under the same conditions.

As shown in Fig. 10, the photodegradation efficiency of CR exceeds 80% in the presence of TiO_2–SA (50 wt %)/PT after four runs of solar light irradiation. On the other hand, the photocatalytic efficiency decreases after each cycle of treatment. The decreased performance in the degradation of CR may be explained by the formation of by-products and their accumulation on the active surface sites of the photocatalyst.

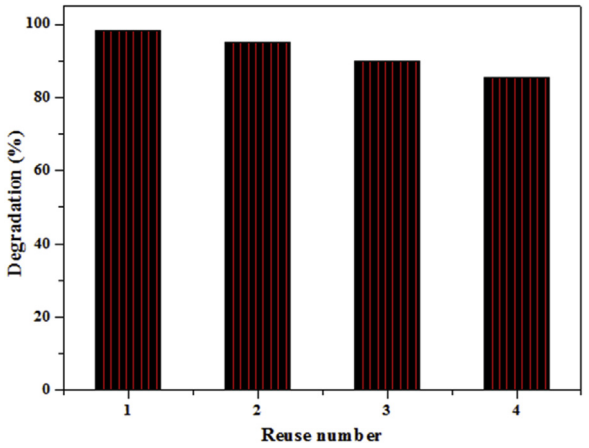

Fig. 10. Effect of reuse number of TiO_2–SA (50 wt %)/PT on the photodegradation of CR after 210 min of solar light irradiation. (Experiments were carried out under solar light irradiation, $T = 34 \pm 2$ °C, volume = 100 mL; pH: natural; initial concentration of CR = 10 mg L^{-1}; catalyst dose = 1.0 g L^{-1}.)

3.11. Photocatalytic tests with other pollutants

To evaluate the photoactivity of the TiO_2–SA (50 wt %)/PT floating photocatalyst with organic pollutants other than CR dye, photodegradation experiments were performed with phenol, 4-nitrophenol, 2.4-dinitrophenol and toluidine. Fig. 11 shows that degradation rates of 58.4, 83.0, 70.7 and 61.6% could be attained for phenol, 4-nitrophenol, 2.4-dinitrophenol and toluidine, respectively. This result shows that the TiO_2–SA (50 wt %)/PT floating photocatalyst has a wide applicability for the removal of organic pollutants from wastewater. Therefore, this novel type of floating photocatalyst will likely trigger a strong interest in this field of research.

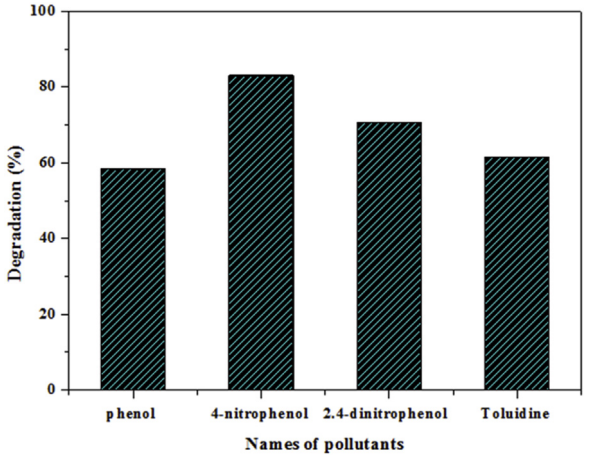

Fig. 11. Photodegradation efficiency of different organic pollutants in the presence of TiO_2–SA (50 wt %)/PT after 210 min. (Experiments were carried out under solar light irradiation, $T = 34 \pm 2$ °C, volume = 100 mL; natural pH; initial concentration of pollutants = 10 mg L^{-1}; catalyst dose = 1.0 g L^{-1}.)

3.12. Possible visible-light-induced photocatalytic mechanism

According to the above experimental research, a probable mechanism for charge transfer and photocatalytic organic dyes over the TiO_2–SA catalyst is suggested and illustrated in Scheme 2. The band gaps of TiO_2 and SA deduced from Fig. 5 are 3.2 eV and 3.97 eV, respectively. The extension of the light absorption of TiO_2–SA to the visible region may be attributed to the synergistic effect between the inorganic and organic composites [40]. The relative energy levels of SA (π and π^* orbitals) and TiO_2 (conduction (CB) and valence (VB) bands) are shown in Scheme 2. According to the experimental results, the mechanism of photocatalytic degradation under solar light irradiation may be interpreted as follows: As a semiconductor material, SA absorbs visible light to induce π–π^* electron transition. Afterward, the excited-state electrons are transported from the π-orbital to the π^*-orbital. The energy levels of the TiO_2 d-orbital (CB) and the SA π^*-orbital match well for the charge transfer [12,41]. So, the excited-state electrons can be readily injected into the CB of TiO_2 and transferred to the nanocomposite surface to react with oxygen and form superoxide radicals $^{\bullet}O_2^-$, subsequently. At the same time, a positive charged hole (h^+) might be formed by electron migration from the TiO_2 valence band to the SA π-orbital, which can react with H_2O in the solution to generate $^{\bullet}OH$. The superoxide radical ion $^{\bullet}O_2^-$ and hydroxyl radical $^{\bullet}OH$ are responsible for the degradation of organic compounds. The whole process is shown and described in Scheme 2.

Therefore, the whole visible-light-induced photocatalytic process of TiO_2–SA can be summarized briefly as follows:

$$TiO_2\text{–}SA + hv \rightarrow TiO_2\text{–}SA^+ + e^- \quad (1)$$

$$TiO_2\text{–}SA^+ \rightarrow TiO_2\text{–}SA + h^+ \quad (2)$$

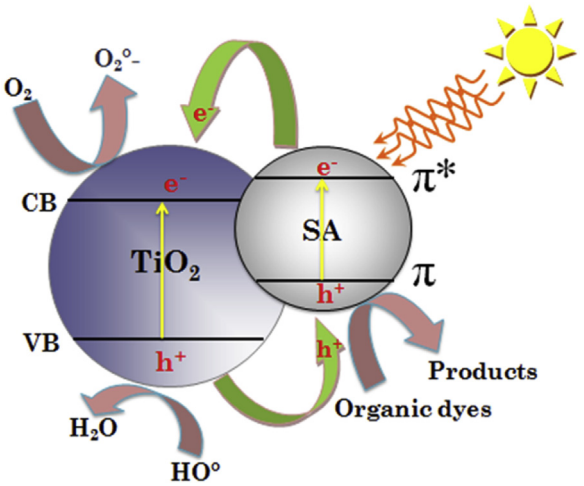

Scheme 2. Mechanism of electron–hole migration under sunlight (e^-: electron; h^+: hole).

$$h^+(H_2O \leftrightarrow H^+ + OH^-) \rightarrow H^+ + {}^\bullet OH \quad (3)$$

$$e^- + O_2 \rightarrow {}^\bullet O_2^- \quad (4)$$

$${}^\bullet O_2^- + CR \rightarrow CR - OO^\bullet \quad (5)$$

$$h_{VB}^+ + CR \rightarrow \text{oxidation of CR} \quad (6)$$

$${}^\bullet OH + CR \rightarrow \text{degradation of CR} \quad (7)$$

Subsequently, large numbers of $^\bullet OH$ and superoxide ($^\bullet O_2^-$) radicals were generated by the decomposition of water (Eq. (3)) and in the presence of O_2 (Eq. (4)). $^\bullet O_2^-$ may form organic peroxides in the presence of organic scavengers (Eq. (5)). While holes in the photocatalyst allow the direct oxidation of CR to reactive intermediates (Eq. (6)) [42], the $^\bullet OH$ radicals allow the degradation of CR to form final decomposition products (Eq. (7)). The recombination process of the electron–hole pairs is then suppressed, and the charge separation and stabilization are reached. Consequently, the efficient electron–hole separation leads to a remarkable enhancement of photocatalytic CR degradation in the presence of TiO_2–SA composite.

4. Conclusion

The results presented in this work have shown that PT can be used to support TiO_2–SA to prepare an active floating photocatalyst. The PT is a natural material, non-toxic and low cost. As a catalyst support, PT offers a good chemical, thermal and mechanical resistance. On the other hand, the obtained results showed that surface modification of TiO_2 nanoparticles by SA via the impregnation method is a facile way to improve its photocatalytic activity under solar light irradiations. The prepared TiO_2–SA/PT floating photocatalyst can be used to remediate waters contaminated with dyes, phenols or other pollutants. It can be recovered and recycled at least four times before losing high activity. The floating photocatalysts have potential applications, such as the treatment of contaminated wastewater reservoirs located in remote areas without any special equipment or installation. In particular, they can be used for the destruction of suspended insoluble organic contaminants, e.g., in oil-spill accidents.

References

[1] C.-S. Hong, Y. Wang, B. Bush, Chemosphere 36 (1998) 1653–1667.
[2] H.M. Coleman, B.R. Eggins, J.A. Byrne, F.L. Palmer, E. King, Appl. Catal. B: Environ. 24 (2000) L1–L5.
[3] Y. Ohko, I. Ando, C. Niwa, T. Tatsuma, T. Yamamura, T. Nakashima, Y. Kubota, A. Fujishima, Environ. Sci. Technol. 35 (2001) 2365–2368.
[4] P. Borker, A.V. Salker, Mater. Sci. Eng. B 133 (2006) 55–60.
[5] A.M. Amat, A. Arques, M.A. Miranda, S. Seguí, Solar Energy 77 (2004) 559–566.
[6] K. Lin, J. Pan, Y. Chen, R. Cheng, X. Xu, J. Hazard. Mater. 161 (2009) 231–240.
[7] H.G. Kim, P.H. Borse, W. Choi, J.S. Lee, Angew. Chem. Int. Ed. 44 (2005) 4585–4589.
[8] M.D. Hernandez-Alonso, F. Fresno, S. Suarez, J.M. Coronado, Energy Environ. Sci. 2 (2009) 1231–1257.
[9] A. Fujishima, X. Zhang, D.A. Tryk, Surf. Sci. Rep. 63 (2008) 515–582.
[10] T. Ochiai, A. Fujishima, J. Photochem. Photobiol. C: Photochem. Rev. 13 (2012) 247–262.
[11] T. Ochiai, Electrochemistry 82 (2014) 720–725.
[12] X. Li, D. Wang, G. Cheng, Q. Luo, J. An, Y. Wang, Appl. Catal. B: Environ. 81 (2008) 267–273.
[13] X. Li, D. Wang, Q. Luo, J. An, Y. Wang, G. Cheng, J. Chem. Technol. Biotechnol. 83 (2008) 1558–1564.
[14] R.L. Narayana, M. Matheswaran, A.A. Aziz, P. Saravanan, Desalination 269 (2011) 249–253.
[15] D. Chen, A.K. Ray, Appl. Catal. B: Environ. 23 (1999) 143–157.
[16] A. Fujishima, T.N. Rao, D.A. Tryk, J. Photochem. Photobiol. C: Photochem. Rev. 1 (2000) 1–21.
[17] L. Shun-Xing, Z. Feng-Ying, C. Wen-Lian, H. Ai-Qin, X. Yu-Kun, J. Hazard. Mater. 135 (2006) 431–436.
[18] L. Shun-Xing, F. Zheng, S. Cai, W. Liang, Y. Li, Sens Actuators B: Chem. 188 (2013) 280–285.
[19] L. Shun-Xing, W. Liang, F. Zheng, X. Lin, J. Cai, Nanoscale 6 (2014) 14254–14261.
[20] L. Shun-Xing, F. Zheng, X. Liu, F. Wu, N. Deng, J. Yang, Chemosphere 61 (2005) 589–594.
[21] M.F. Nsib, A. Maayoufi, N. Moussa, N. Tarhouni, A. Massouri, A. Houas, Y. Chevalier, J. Photochem. Photobiol. A: Chem. 251 (2013) 10–17.
[22] L.C.R. Machado, C.B. Torchia, R.M. Lago, Catal. Commun. 7 (2006) 538–541.
[23] S. Lan, L. Liu, R. Li, Z. Leng, S. Gan, Ind. Eng. Chem. Res. 53 (2014) 3131–3139.
[24] Q. Geng, W. Cui, Ind. Eng. Chem. Res. 49 (2010) 11321–11330.
[25] S. Liufu, H. Xiao, Y. Li, J. Colloid Interface Sci. 281 (2005) 155–163.
[26] H. Hidaka, H. Honjo, S. Horikoshi, N. Serpone, Catal. Commun. 7 (2006) 331–335.
[27] W. Macyk, K. Szaciłowski, G. Stochel, M. Buchalska, J. Kuncewicz, P. Łabuz, Coord. Chem. Rev. 254 (2010) 2687–2701.
[28] A.D. Weisz, L. García Rodenas, P.J. Morando, A.E. Regazzoni, M.A. Blesa, Catal. Today 76 (2002) 103–112.
[29] A.D. Weisz, A.E. Regazzoni, M.A. Blesa, Solid State Ionics 143 (2001) 125–130.
[30] K.D. Dobson, A.J. McQuillan, Spectrochim. Acta Part A: Mol. Biomol. Spectrosc. 56 (2000) 557–565.
[31] G. Cao, Y. Li, Q. Zhang, H. Wang, J. Hazard. Mater. 178 (2010) 440–449.
[32] M. Ye, Z. Chen, W. Wang, J. Shen, J. Ma, J. Hazard. Mater. 184 (2010) 612–619.
[33] Y. Yu, M.-Z. Zhang, J. Chen, Y.-D. Zhao, Dalton Trans. 42 (2013) 885–889.
[34] J. Fernández, J. Kiwi, J. Baeza, J. Freer, C. Lizama, H.D. Mansilla, Appl. Catal. B: Environ. 48 (2004) 205–211.
[35] N. Daneshvar, D. Salari, A.R. Khataee, J. Photochem. Photobiol. A: Chem. 157 (2003) 111–116.
[36] T. Ohno, Y. Masaki, S. Hirayama, M. Matsumura, J. Catal. 204 (2001) 163–168.
[37] X. Li, C. Chen, J. Zhao, Langmuir 17 (2001) 4118–4122.
[38] I.K. Konstantinou, T.A. Albanis, Appl. Catal. B: Environ. 49 (2004) 1–14.
[39] N.M. Mahmoodi, M. Arami, N.Y. Limaee, N.S. Tabrizi, J. Colloid Interface Sci. 295 (2006) 159–164.
[40] D. Wang, J. Zhang, Q. Luo, X. Li, Y. Duan, J. An, J. Hazard. Mater. 169 (2009) 546–550.
[41] S. Mu, Y. Long, S.-Z. Kang, J. Mu, Catal. Commun. 11 (2010) 741–744.
[42] S.K. Kansal, M. Singh, D. Sud, J. Hazard. Mater. 141 (2007) 581–590.